Uniform orientation and size of ferroelectric domains

D. Yadlovker and S. Berger

Faculty of Materials Science and Engineering, Technion, Haifa 32000 Israel
(Received 18 December 2004; published 27 May 2005)

Rochelle salt (RS) ($NaKC_4H_4O_6 \cdot 4H_2O$) single crystals were grown inside an array of alumina pores having an average diameter of 30 nm and length of about 0.5 μm. The crystals have a monoclinic crystallographic structure and uniform crystallographic orientation. High-resolution transmission electron microscopy vertical cross section images show multiple nanometer-sized 180° ferroelectric domains in each single crystal having uniform size and orientation along the longitudinal axis of the pores. The nanodomain boundaries consist of a single crystallographic plane of a rotation twin. This configuration of ferroelectric nanodomains results in enhanced polarization, which is higher by one order of magnitude than the maximum polarization values reported for bulk-size RS crystals. The pores stabilize the ferroelectric phase up to 55 °C (decomposition temperature of RS), which is higher by about 30 °C relative to the upper transition temperature of bulk-size RS crystals. The highly dense array of individual ferroelectric single crystals with uniform polarization orientation and size of nanodomains, as presented in this paper, is a basis for future high-resolution and high-density ferroelectric-based devices, where each nanocrystal inside a pore can serve as a detector, sensor, or actuator.

I. INTRODUCTION

The subject of nanoferroelectric domains has gained much attention during recent years, motivated by a desire for miniaturization of ferroelectric-based devices. Two critical values mark a pronounced effect of grain size on ferroelectric behavior.[1,2] The first one, which occurs in the submicrometer size range, indicates the transition from multidomain to single-domain grains. The second one, which occurs in the nanometer size range, marks the transition from a single-domain to a nonferroelectric phase. Various values of this critical size were reported experimentally, even for the same material, since it depends on many parameters such as microstructure, composition, defects, stress, and the quality of interfaces with conductive electrodes; for example, 49 nm in $BaTiO_3$ thin films,[3] 3 nm in $BaTiO_3$ thin films under high tensile stress,[4] 30 nm in $BaTiO_3$ powder particles,[5] 7–14 nm in $PbTiO_3$ thin films,[6,7] and 4 nm in $Pb(Zr_{0.25}Ti_{0.75})O_3$ thin films.[8] These examples demonstrate that few nanometer-thick ultrathin ferroelectric films can be applied in ferroelectric-based devices. The presence of nanodomains in ultrathin films has been confirmed experimentally. Recent studies have shown, by the x-ray diffraction (XRD) technique, 180° stripe domains having a width of 3.7–24 nm in ultrathin $PbTiO_3$ films,[9] and by the high-resolution transmission electron microscopy (HRTEM) technique, 180° domains having a width of 0.4–1.2 nm in ultrathin $BaTiO_3$ films.[4] However, the challenge of controlling the size and orientation of ferroelectric nanodomains, which is essential for future ferroelectric-based nanodevices, has not been accomplished yet.

This paper demonstrates a method of controlling the orientation and size of ferroelectric nanodomains, which is based on controlled nucleation and growth of single crystals inside a highly dense array (about 10^{11} cm^{-2}) of alumina nanopores, having an average diameter of about 30 nm. The single crystals are grown with uniform crystallographic orientation, which is the main polarization direction of the ferroelectric phase, along the longitudinal axis of the pores. Nanodomains are formed in each single crystal according to its crystallographic orientation and size, and the structure, composition, and surface energy of the pore walls. The highly dense array of individual ferroelectric single crystals with uniform polarization orientation and size of nanodomains, as presented in this paper, is a basis for future high-resolution and high-density ferroelectric-based devices,
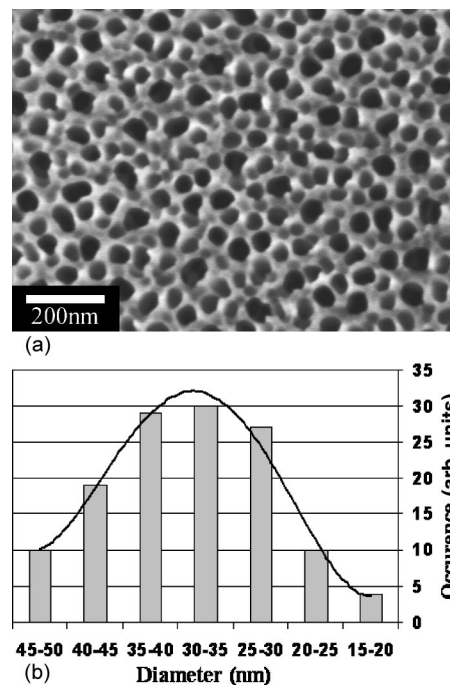

(a)

(b)

FIG. 1. (a) HRSEM top-view image of pores grown on electrochemically polished pure aluminum substrate at 25°. (b) Size distribution of the alumina pores determined from the HRSEM image.
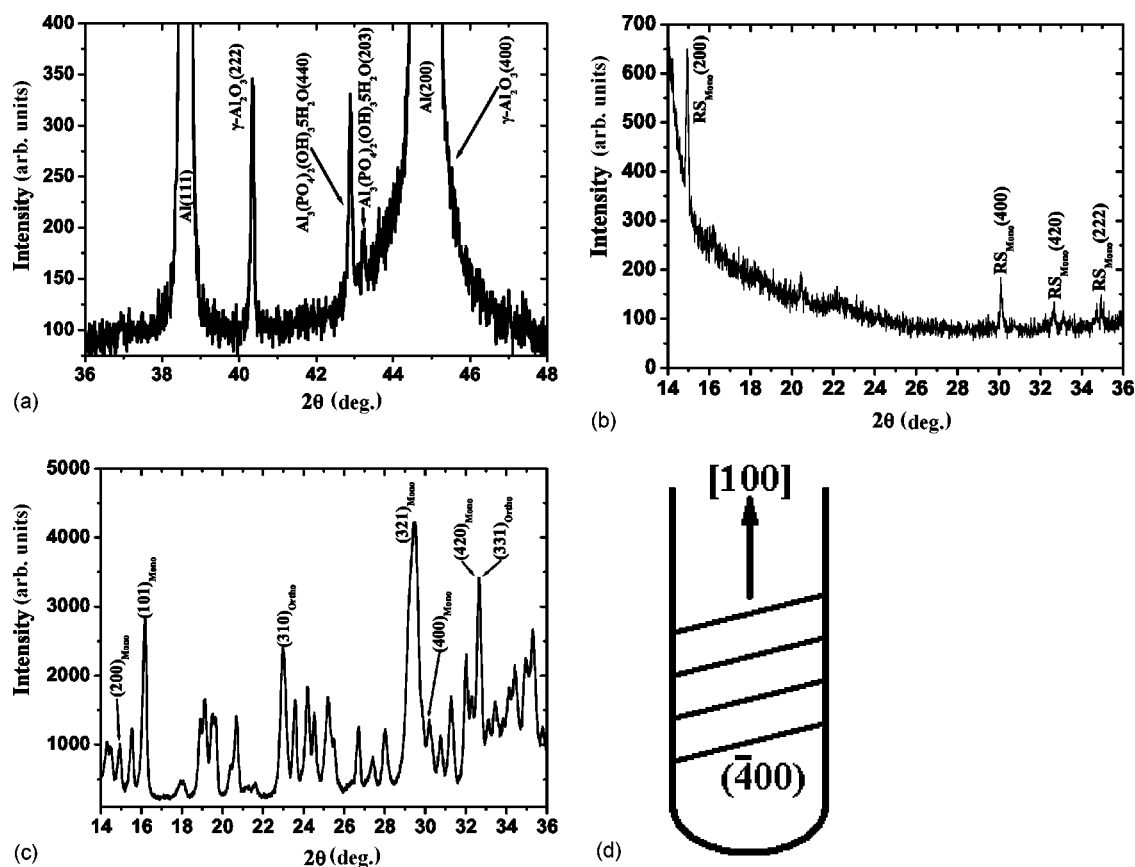
FIG. 2. XRD spectra of (a) the empty porous film; (b) the RS-filled porous film; (c) the RS polycrystalline powder; (d) a schematic description of the [100] crystallographic orientation and ($\bar{4}$00) planes of the RS crystals inside the alumina pores.

where each nanocrystal inside a pore can serve as a detector, sensor, or actuator.

II. EXPERIMENT

Thin porous alumina films (about 0.5 μm thick) were formed on the surface of pure aluminum foils (0.5 mm thick) by electrochemical anodization. Prior to anodization, the Al surface was electropolished to a high degree of smoothness using an electrolyte solution of perchloric acid and ethanol (3:7 volume ratio) under a constant potential at 25 °C. The anodization was done in an aqueous phosphoric solution (3 vol %) under a constant current density at 25 °C. The anodized samples were inserted into a saturated aqueous solution of Rochelle salt (RS) [prepared by dissolution of pure RS (NaKC$_4$H$_4$O$_6$·4H$_2$O) powder in deionized water at 40 °C]. After a few minutes the liquid solution was cooled down to about 25 °C leading to precipitation of RS crystals from the supersaturated solution to the anodized surface. The cooling process was done slowly at a rate of about 0.25 °C min^{-1} to enable nucleation and growth of single crystals in the pores. After a few hours the samples were pulled out from the solution and dried at 25 °C under controlled humidity for 1 week. Finally, the RS crystals outside the pores were removed by wiping delicately the surface of the porous film with a moist cloth.

The surface morphology of the porous films was characterized using a high-resolution scanning electron microscopy (HRSEM) operated at the in-lens mode and low voltages (1.5–4 kV). Composition elemental analysis was performed on the surface of the RS-filled porous film using wavelength dispersion spectroscopy (WDS). The crystallographic structures of the films were identified using the Bragg-Brentano XRD method operated at a range of angles between 10° and 50°, which covers the main peaks of the RS (15°–35°) and the alumina pore walls (35°–50°). The XRD beam covers a rectangular surface area of about 20×5 mm^2, which contains about 10^{11} pores, and penetrates to a depth of about 1 μm, which covers the entire thickness of the porous film. The microstructure of the RS inside the pores was characterized by observing vertical cross section samples with high-resolution TEM. Ferroelectric measurements were done vertical to the porous film plane. The top Al contacts (3 mm diameter) were deposited on the surface of the empty and RS-filled porous films. The Al surface at the back side of the sample was used as a bottom electrode. The top and bottom electrodes were connected with conductive wires to the modified Sawyer-Tower circuit[10] for measuring polarization hysteresis curves at temperatures between 21 and 60 °C. Based on these measurements the following characteristics of the RS-filled film were determined: spontaneous polarization, remanent polarization, coercive field, and thermal stability of the ferroelectric phase. The switching time of the RS
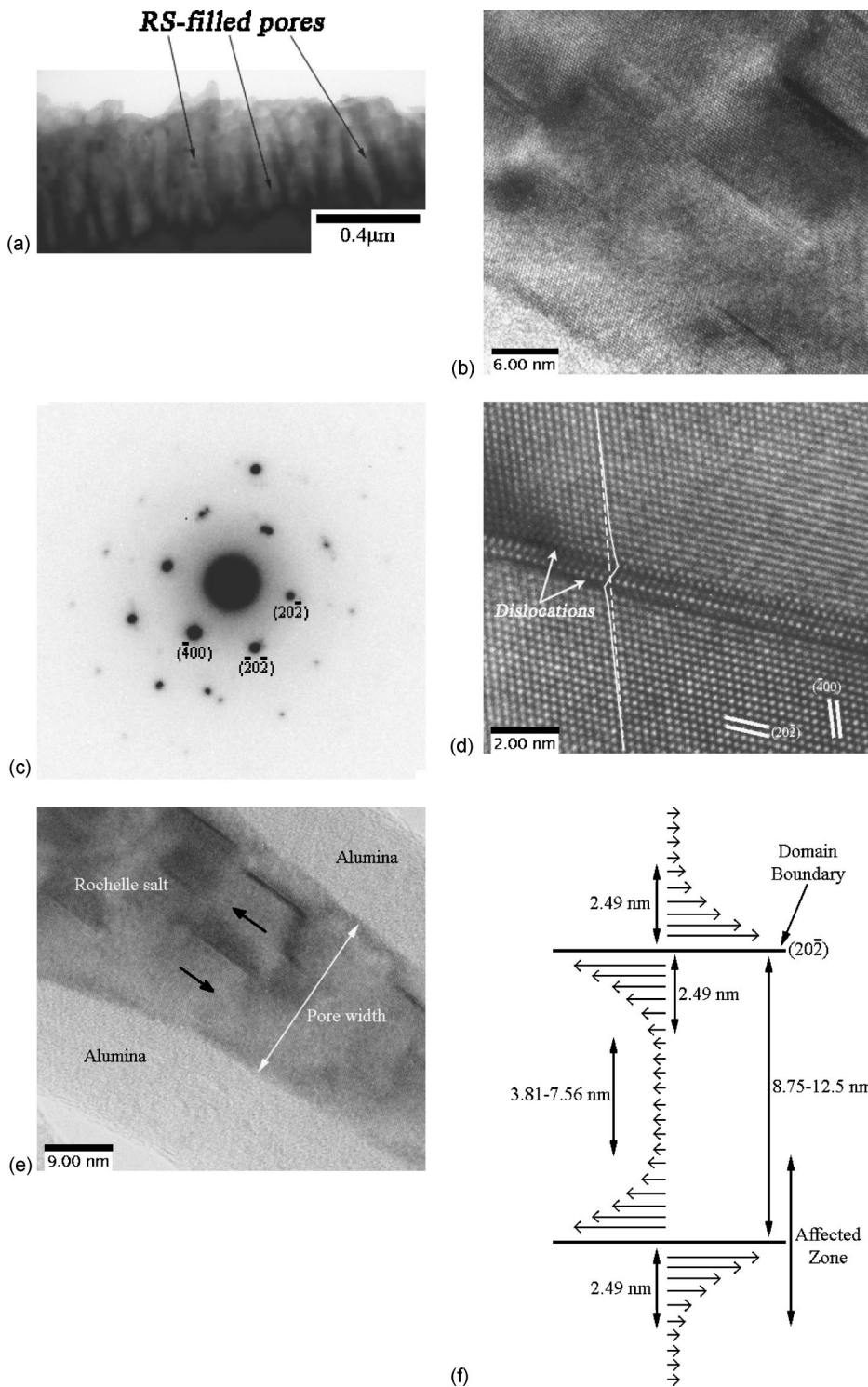
FIG. 3. (a) A TEM vertical cross section image of the alumina pores filled with RS. (b) Electron diffraction pattern taken from a vertical cross section area that contains 25 pores. (c) A lattice image showing a single RS crystal in a pore. (d) A magnified lattice image of the RS single crystal in the pore, showing defects (darker lines) having uniform size and orientation. (e) A lattice image that shows a nanodomain boundary at each darker line, which consists of a single $(20\bar{2})$ plane and 180° symmetric shear movements of atoms on both sides of the domain boundary, indicated by continuous lines drawn on the atoms of a single row relative to their equilibrium positions (dashed line). (f) A schematic illustration of the shear movements of atoms on both sides of the domain boundary toward the [100] direction along the longitudinal axis of the pore.

ferroelectric domains in the pores was determined by measuring the difference in the rise time of a square voltage pulse (1–5 V) at 1 kHz and 21 °C.[11]

III. RESULTS AND DISCUSSION

HRSEM images of the electrochemically anodized Al surface show [e.g., Fig. 1(a)] a continuous porous film that contains a highly dense array of pores (about 10^{11} cm^{-2}). The

pores uniformly cover the anodized surface with a narrow size distribution between 20 and 40 nm [Fig. 1(b)]. After filling the pores with RS, no empty pores were observed while scanning a large area (about 80 μm^2) of the surface with a HRSEM. WDS measurements verified the presence of sodium and potassium elements and no contaminant elements in the porous film.

The XRD spectrum of the empty porous film [Fig. 2(a)] shows the presence of two phases: γ-alumina and aluminum
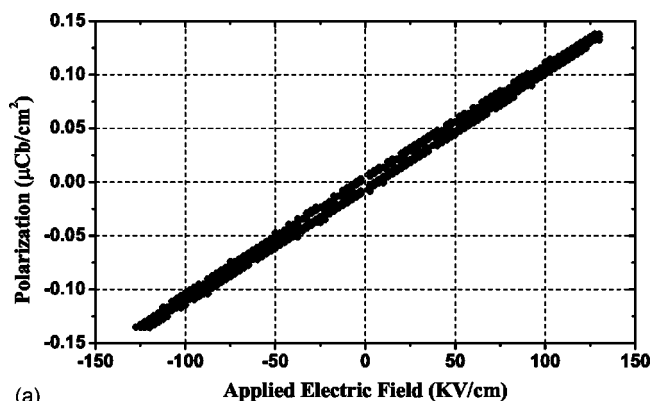
(a)
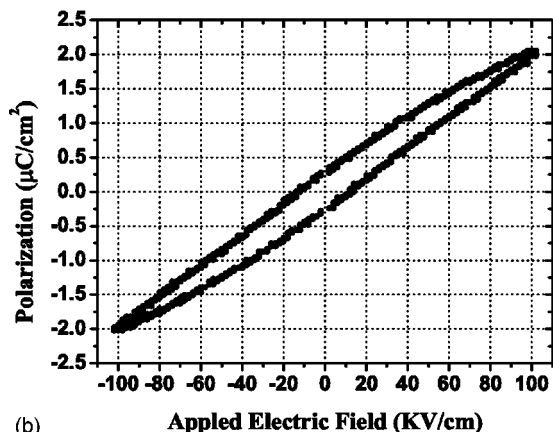
(b)

FIG. 4. Polarization vs applied electric field measured at 1 kHz and 21 °C for (a) empty porous alumina; (b) RS-filled porous alumina.

FIG. 5. Switching time vs applied electric field measured at 1 kHz and 21 °C for RS-filled porous alumina.

phosphate hydroxide hydrate. These phases are characteristic to porous alumina film prepared by electrochemical anodization in a phosphoric-based electrolyte.[12,13] The XRD spectrum of the RS-filled porous film [Fig. 2(c)], shows only a few peaks, which are associated with the RS. In the literature, there is only one JCPDS card for the RS, which corresponds to the orthorhombic paraelectric phase.[14] We calculated the expected positions (angels) of XRD peaks of the RS monoclinic phase based on the data for the unit cell and positions of atoms.[15] It turns out that the XRD peaks of the monoclinic phase are positioned close to those of the orthorhombic phase but they can be identified with the peaks of the {400} and {200} crystallographic planes (a difference of about 0.2% between the two phases). According to this information, the XRD peaks of the RS in the porous film correspond only to the monoclinic phase. The intensity of the (200) peak is higher by at least one order of magnitude compared to the other RS peaks, indicating a preferred crystallographic orientation of the RS crystals in the pores toward the [100] direction. The measurement geometry is such that the [100] direction of the RS crystals is along the longitudinal axis of the pores [Fig. 2(d)]. The experimental reference for determining the preferred crystallographic orientation of the RS crystals in the pores was the XRD spectrum of randomly oriented RS polycrystals [Fig. 2(b)] in a powder, which was prepared from the same liquid solution used for filling the pores.
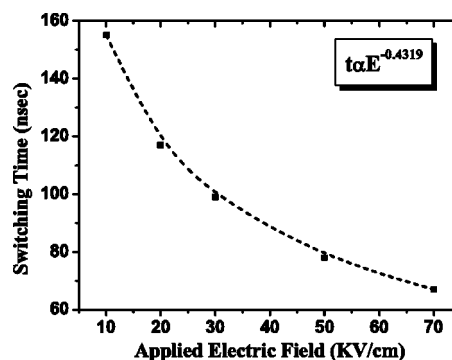
TEM vertical cross section bright field images of the RS-filled porous film show [Fig. 3(a)] the vertical orientation of the pores relative to the film plane, the size uniformity, and the continuity of the pores to the entire depth of the film (about 0.5 μm). The electron diffraction pattern taken from the film (a selected vertical cross section area that contains about 25 pores) reveals dot patterns characteristic of the monoclinic phase of RS crystals [Fig. 3(b)]. The dot patterns correspond to a single zone axis ([010]), indicating the uniform crystallographic orientation of the RS crystals in the pores, as observed in the XRD spectrum. HRTEM lattice images [e.g., Fig. 3(c)] show that each pore contains a single crystal of RS, which completely fills the pore volume, and the lattice lines, which correspond to the $(20\bar{2})$ planes, are aligned along the longitudinal axis of the pores. The HRTEM images also show darker lines in the RS crystals, which are oriented only toward the longitudinal axis of the pore and have a width of about 1 nm and length of about 10 nm [Figs. 3(c) and 3(d)]. A magnified lattice image of these lines shows [Fig. 3(e)] a structural defect that consists of a shear displacement of atoms on neighboring $(20\bar{2})$ planes along the [100] direction, which is ended by dislocations at the edges of the line [marked on Fig. 3(e)]. This structural defect corresponds to a rotation twin, which has a 180° rotation symmetry relative to the [010] direction (this direction is vertical to the lattice image plane). The lattice image also reveals a decrease of shear displacement of atoms with increasing dis-
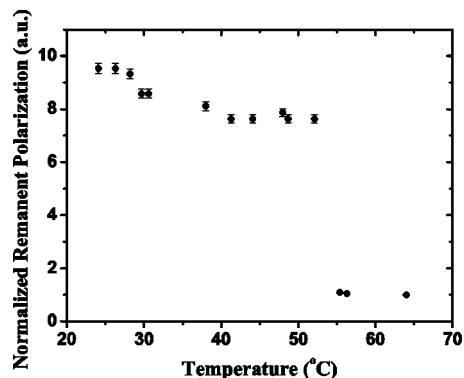

FIG. 6. Normalized remanent polarization of RS-filled pores vs temperature at 1 kHz, and applied electric field of 30 kV/cm.

tance from the defect center until a distance of four interplanar spacing of $(20\bar{2})$ planes (2.49 nm), where the position of the atoms returns to about their regular order [e.g., Fig. 3(e)]. The displacement of atoms on one side of the defect center toward the [100] direction, which is the main polarization direction in the RS monoclinic phase, creates electric dipoles oriented in the same direction, which is a ferroelectric domain. The displacement of the atoms on the other side of the defect center creates also a ferroelectric domain, which is oriented at 180° relative to that in the first side of the defect. The boundary between the 180° ferroelectric domains is a $(20\bar{2})$ plane, oriented toward the [100] crystallographic direction, that separates the two regions where shear displacement occurred [Fig. 3(e)]. Bulk-size RS crystals have the same type of ferroelectric domain (only 180°) and the same domain-boundary orientation ([100]).[16] The width of the nanodomains is restricted to the distance between neighboring defect lines, which is about 8–13 nm. The length of the domains is equal to the length of the defect line, which is about 7–12 nm. The lattice image [Fig. 3(c) and 3(d)] clearly shows multiple defect lines separating 180° nanodomains in the RS single crystal, which are all aligned along the longitudinal axis of the pore and have about the same size [schematically illustrated in Fig. 3(f)].

Dielectric measurements of the empty porous film at 1 kHz and 21 °C show a linear dependence of polarization on the applied electric field [Fig. 4(a)], dielectric constant of about 8, high electrical resistivity of about 3.3×10^7 Ω cm, and quality factor of about 10. These dielectric properties correspond to the alumina pore walls. The dielectric measurements of the RS-filled porous film show [Fig. 4(b)] a nonlinear dielectric behavior characterized by a polarization hysteresis loop, remanent polarization, and coercive field of about 0.28 μC cm^{-2} and 13 kV cm^{-1}, respectively. The measured polarization of about 2.0 μC cm^{-2} at 100 kV cm^{-1} is higher by one order of magnitude compared to saturated polarization values reported for bulk-size RS crystals.[10] This polarization enhancement is attributed to a higher density of domain walls in the nanocrystals as observed in HRTEM images [e.g., Figs. 3(c) and 3(d)]. The polarization increases with increasing density of domain boundaries according to the known domain-wall motion mechanism. The measured value of the coercive field, which is higher by a factor of about 65 compared to reported values of nonrestrained bulk-size RS crystals,[10] indicates the relatively high difficulty of reversing the polarization direction of the nanodomains within the confined volume of the pores. The switching time of the RS nanodomains in the pores, which is in the range of 60 to 160 ns under an applied electric field of 70–10 kV cm^{-1}, respectively (Fig. 5), decreases with increasing applied electric field according to a power law dependence as expected from domain-wall movements.[11] *In situ* measurements of polarization as a function of temperature during heating show (Fig. 6) that the RS crystals in the pores exhibit a ferroelectric behavior continuously from 21 up to about 55 °C, which is higher by about 30 °C above the upper transition temperature of bulk-size RS crystals.[16] This result indicates that the pore walls stabilize the ferroelectric monoclinic phase of the RS crystals, probably due to electrostatic interactions between polar bonds. The relatively small loss (about 20%) of remanent polarization between 25 and 40 °C (Fig. 6) is attributed to thermal annealing of some of the nanodomain boundaries, which are located "far" from the pore walls and are therefore less affected by their electrostatic forces. The major and sharp fall of the remanent polarization at about 55 °C is attributed to the decomposition of RS crystals into sodium tartrate and potassium tartrate as observed for bulk-size RS crystals;[16] which means that the RS crystals in the pores maintain the ferroelectric behavior up to their decomposition temperature, which is not affected by the pore walls.

IV. SUMMARY

Rochelle salt single crystals were grown inside pores having an average diameter of 30 nm and length of about 0.5 μm. The crystals have the monoclinic crystallographic structure and uniform orientation of [100] along the longitudinal axis of the pores. Their formation requires nucleation at the bottom of the pores and preferred growth due to a tight control on various parameters such as temperature and composition. Nanometer-size 180° ferroelectric domains were observed, by HRTEM studies, in the RS crystals, which are uniformly oriented along the longitudinal axis of the pores. Each domain boundary consists of a single crystallographic plane of a rotation twin. The presence of multiple nanodomains with uniform orientation along the direction of applied electric field results in enhanced polarization values, which are higher than those reported for bulk-size RS crystals. The pores stabilize the ferroelectric phase of the crystals until their decomposition temperature. The formation of a highly dense array of ferroelectric single crystals, having uniform size and crystallographic and domain orientation, as presented in this paper, is the initial step toward the development of ferroelectric-based sensors and detectors with nanometer-size lateral resolution.

[1] G. Arlt, J. Mater. Sci. **25**, 2655 (1990).

[2] R. E. Newnham and S. Trolier-McKinstry, Integr. Ferroelectr. **20**, 1 (1998).

[3] S. Schlag and H. F. Eicke, Solid State Commun. **91**, 883 (1994).

[4] Y. Drezner and S. Berger, J. Appl. Phys. **94**, 6774 (2003).

[5] H. I. Hsiang and F. S. Yen, J. Am. Ceram. Soc. **79**, 1053 (1996).

[6] S. Chattopadhyay, P. Ayyub, V. R. Palkar, and M. Multani, Phys. Rev. B **52**, 13177 (1995).

[7] W. L. Zhong, B. Jiang, P. L. Zhang, J. M. Ma, H. M. Cheng, Z. H. Yang, and L. X. Li, J. Phys.: Condens. Matter **5**, 2619 (1993).

[8] T. Tybell, C. H. Ahn, and J.-M Triscone, Appl. Phys. Lett. **75**, 856 (1999).

⁹S. K. Streiffer, J. A. Eastman, D. D. Fong, C. Thompson, A. Munkholm, M. V. Ramana Murty, O. Auciello, G. R. Bai, and G. B. Stephenson, Phys. Rev. Lett. **89**, 067601 (2002).

¹⁰C. B. Sawyer and C. H. Tower, Phys. Rev. **35**, 269 (1930).

¹¹J. F. Scott, *Ferroelectric Memories* (Springer-Verlag, Berlin, 2000), Chap. 6, p. 121.

¹²G. E. Thompson, and G. C. Wood, Nature (London) **290**, 230 (1981).

¹³G. E. Thompson, R. C. Furneaux, G. C. Wood, J. A. Richardson, and J. S. Goode, Nature (London) **272**, 433 (1978).

¹⁴JCPDS Powder Diffraction File No. 29-1046, 1988 (unpublished).

¹⁵E. Suzuki, and Y. Shiozaki, Phys. Rev. B **53**, 5217 (1996).

¹⁶F. Jona, and G. Shirane, *Ferroelectric Crystals* (Pergamon Press, New York, 1961), Chap. VII, p. 281.